

CrossMark
click for updatesCite this: *RSC Adv.*, 2015, 5, 33632

Transport properties of g-BC₃ and t-BC₃ phases

A. H. Reshak^{*ab}

The calculated electronic band structure shows that the g-BC₃ phase is a narrow band gap semiconductor constructed from an ABAB,..., stacking sequence. Whereas t-BC₃ is a metallic phase constructed from a sandwich-like metal-insulator lattice from an alternately stacking sequence of a metallic CBC block and an insulating CCC block. The electronic transport coefficients of the g-BC₃ and t-BC₃ phases are obtained with the aid of the semi-classical Boltzmann theory and the rigid band model based on density functional theory within the recently modified Becke–Johnson potential (mBJ). The semiconductor phase (g-BC₃) exhibits a linearly dependent charge carrier concentration and electrical conductivity with temperature, whereas for the t-BC₃ phase the charge carrier concentration is increased with increasing temperature up to 200 K, then a rapid decrease occurs upon increasing the temperature. The electrical conductivity of t-BC₃ shows the highest value at 50 K then a rapid decrease occurs upon increasing the temperature up to 250 K, and it stays roughly constant above this temperature. The Seebeck coefficient of the g-BC₃ and t-BC₃ phases shows that these materials exhibit p-type conduction and the g-BC₃ phase exhibits a higher Seebeck coefficient than the t-BC₃ phase. The g-BC₃ phase exhibits an almost linearly dependent power factor with temperature. Whereas the power factor of the t-BC₃ phase shows a very high value at low temperature then drops to the lower value at 200 K. Above this temperature the power factor of t-BC₃ becomes zero along the whole temperature range. It has been found that the g-BC₃ phase shows a higher power factor than that of the t-BC₃ phase. The electronic thermal conductivity of g-BC₃ exponentially increases with increasing temperature. It has a zero value at 50 K and the highest value 4.6×10^{14} (W m⁻¹ K⁻¹ s⁻¹) at 900 K. t-BC₃ exhibits linearly dependent electronic thermal conductivity with temperature. At low temperature (50 K) the electronic thermal conductivity of t-BC₃ is about 0.15×10^{16} (W m⁻¹ K⁻¹ s⁻¹) while it has a value of about 2.1×10^{16} (W m⁻¹ K⁻¹ s⁻¹) at 900 K. It is clear that the g-BC₃ phase exhibits lower electronic thermal conductivity than the t-BC₃ phase.

Received 13th January 2015

Accepted 27th March 2015

DOI: 10.1039/c5ra00746a

www.rsc.org/advances

1. Introduction

Thermoelectric power generators can convert heat into electricity which is a good alternative solution for energy and environmental problems.¹ Ever since this discovery, extensive studies have been done on several materials to enhance their thermoelectric properties for technological applications.^{2–11} The development of novel thermoelectric materials has attracted a great deal of interest due to their significant potential applications ranging from clean energy to photon sensing devices. The efficient thermoelectric materials can be classified into three types; complex crystals, alloys and nano-crystals.¹² They can provide a significant contribution to solve the global sustainable energy problems. The thermoelectric materials may also be used as solid-state Peltier coolers¹² in addition to generating electricity from waste heat. Efficient thermoelectric materials should possess high figure of merit ($ZT = S^2\sigma T/\kappa$), to achieve

this we need to optimize the Seebeck coefficient (S) and electrical conductivity (σ) and lower the thermal conductivity (κ). In recent years thermoelectric materials have played an important role in global sustainable energy solutions.^{13–15}

The growing demand for unusual thermoelectric materials motivated us to comprehensively investigate the transport properties of boron-rich diamond materials. There is great interest in boron-rich diamond materials due to their excellent chemical and physical properties. It has been found that these materials possess high mechanical strength, high hardness, high thermal conductivity, high electron and hole mobility, high chemical inertness, and low mass density.^{16,17} These superhard materials are of great demand for numerous applications for instances in electronic industry, solar cells production and mechanical machining. Several researchers focus their attention on finding novel superhard materials with good conductivity.^{17–24} Combining between superhard and metallic properties are of great interest for the creation multifunctional materials with potential applications as metal-insulator junction, metal-insulator devices and photonic devices.²⁰ It has been reported that the t-BC₃ phase is stable with space group $P\bar{4}2m$,²¹ and exhibits metallic behavior at ambient and high pressures.

^aNew Technologies – Research Centre, University of West Bohemia, Univerzityni 8, 306 14 Pilsen, Czech Republic. E-mail: maalidph@yahoo.co.uk; Tel: +420 777729583

^bCenter of Excellence Geopolymer and Green Technology, School of Material Engineering, University Malaysia Perlis, 01007 Kangar, Perlis, Malaysia

While $g\text{-BC}_3$ is a semiconductor at both ambient and high pressures and stable with space group $Cmcm$.¹⁷ Liu *et al.*¹⁷ predicted the synthesis of the $t\text{-BC}_3$ phase from $g\text{-BC}_3$ phase at high pressure and they confirm the stability of both phases at the space group $P42m$ and $Cmcm$, respectively. Also it was reported that a superconductivity was found in boron-doped diamond synthesized at high temperature and high pressure²⁵ and increasing the dopant concentrations led to enhance the superconductivity.^{26–28}

From above, it is clear that the previous experimental and theoretical work are devoted on the synthesis of BC_3 , study the crystal structure, electronic properties, elastic properties with very few reports on the linear optical properties, all the previous calculations are done using non-full potential methods. Therefore, due to a lack information regarding the thermoelectric properties of the superhard metallic $g\text{-BC}_3$ and $t\text{-BC}_3$ compounds, and as natural extended to our recent work on $g\text{-BC}_3$ and $t\text{-BC}_3$ (ref. 29) we have addressed ourselves for comprehensive theoretical calculations based on the density functional theory (DFT) within all-electron full potential method and the semi-classical Boltzmann theory as incorporated in BoltzTraP code³⁰ to calculate the thermoelectric properties of $g\text{-BC}_3$ and $t\text{-BC}_3$ phases. In this calculation we have employed the all-electron full potential linear augmented plane wave plus local orbitals (FP-LAPW + lo) method. First-principles calculation is one strong and useful tool to predict the crystal structure and its properties related to the electron configuration of a material before its synthesis.^{31–34}

2. Details of calculations

The graphitic-like $g\text{-BC}_3$ crystallizes in orthorhombic space group $Cmcm$, with ABAB, ..., stacking sequence as illustrated in Fig. 1(a). In the unit cell of $g\text{-BC}_3$ the structural parameters are $a = 8.834 \text{ \AA}$, $b = 5.104 \text{ \AA}$ and $c = 7.071 \text{ \AA}$, the B atom is located at (0.167, 0.823, 0.25), C1 at (0.159, 0.323, 0.25), C2 at (0.792, 0.562, 0.25) and C3 at (0.421, 0.585, 0.25).¹⁷ The boron-rich diamond $t\text{-BC}_3$ crystallizes in tetragonal space group $P42m$ with eight atoms per unit cell as illustrated in Fig. 2(a–d). The structural parameters of $t\text{-BC}_3$ are $a = b = 3.513 \text{ \AA}$ and $c = 3.871 \text{ \AA}$, the B atom is situated at (0.5, 0.0, 0.5), C1 at (0.0, 0.0, 0.0), C2 at (0.25, 0.25, 0.229) and C3 at (0.5, 0.5, 0.0).¹⁷ In both ($t\text{-BC}_3$ and $g\text{-BC}_3$) phases the B atom connected to three C atoms in different configurations.

Using the all-electron full potential linear augmented plane wave plus local orbitals (FP-LAPW + lo) method as implemented in WIEN2k code³⁵ within generalized gradient approximation (PBE-GGA),³⁶ the geometry of $t\text{-BC}_3$ and $g\text{-BC}_3$ are relaxed by minimizing the forces acting on each atom. The structures are totally relaxed when the forces on each atom reach values less than 1 mRy per a.u. From the relaxed geometry the ground state properties of $t\text{-BC}_3$ and $g\text{-BC}_3$ are calculated within the local density approximation (CA-LDA),³⁷ PBE-GGA and Engel–Vosko generalized gradient approximation (EVGGA).³⁸ To overcome the DFT-LDA/GGA band gap's underestimation we have introduced EVGGA. It is well known that EVGGA able to reproduce better exchange potential at the expense of less agreement in

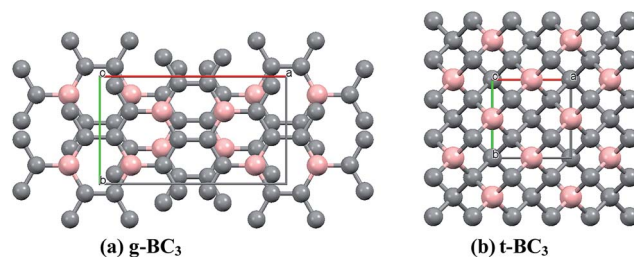


Fig. 1 (a) Fragment of the crystal structure of $g\text{-BC}_3$ phase which has ABAB stacking sequence; (b) fragment of the crystal structure of $t\text{-BC}_3$ phase which is constructed by two different building blocks, these are CCC (composed of two C sheets) and CBC (composed of one B sheet and one C sheet). These building blocks form sandwich-like layered structure with alternately stacking sequences of atomic planes C–C–B–C–C–C–B–C–C (a sandwich-like conducting super-hard boron carbide). The B is represented by pink color and C atom by gray color.

the exchange energy. This approach yields better band splitting compared to LDA and GGA but still underestimated the band gap therefore, we have used the recently modified Becke–Johnson potential (mBJ).³⁹ The mBJ, a modified Becke–Johnson potential, allows the calculation of band gaps with accuracy similar to the very expensive GW calculations.³⁹ It is a local approximation to an atomic “exact-exchange” potential and a screening term. We should mention that hybrid functionals^{40,41} are a correct way of solving the under-estimated band gaps that they observe in the boron/carbon structures.

The plane-wave cutoff, defined by the product of the smallest atomic sphere radius times the magnitude of the largest reciprocal-lattice vector ($R_{\text{MT}} \times K_{\text{MAX}}$), is taken to be equal to 8. In the muffin-tin (MT) spheres the potential and charge density are expanded in spherical harmonics with $l_{\text{max}} = 8$ and nonspherical components up to $l_{\text{max}} = 6$. In the interstitial region the potential and the charge density are represented by Fourier series. Self-consistency is obtained using 800 \vec{k} points in the irreducible Brillouin zone (IBZ). We have calculated the transport properties using 12 000 \vec{k} points in the IBZ. The convergence of the total energy in the self-consistent calculations is taken with respect to the total charge of the system with a tolerance 0.0001 electron charges. We have used the semi-classical Boltzmann theory as incorporated in BoltzTraP code³⁰ to calculate the thermoelectric properties like carrier concentration (n), Seebeck coefficient (S), electrical conductivity (σ/τ), electronic thermal conductivity (κ_e/τ), and the electronic power factor ($S^2\sigma/\tau$) as a function of temperature at certain value of the chemical potential. The constant relaxation time approximation and the rigid band approximation were used in the calculations.³⁰ BoltzTrap code depends on a well tested smoothed Fourier interpolation to obtain an analytical expression of bands. This is based on the fact that the electrons contributing to transport are in a narrow energy range due to the delta-function like Fermi broadening. For such a narrow energy range the relaxation time is nearly the same for the electrons. The accuracy of this method has been well tested earlier, and the method actually turns out to be a good approximation.⁴² The temperature dependence of the energy band structure is ignored. The formula of the transport

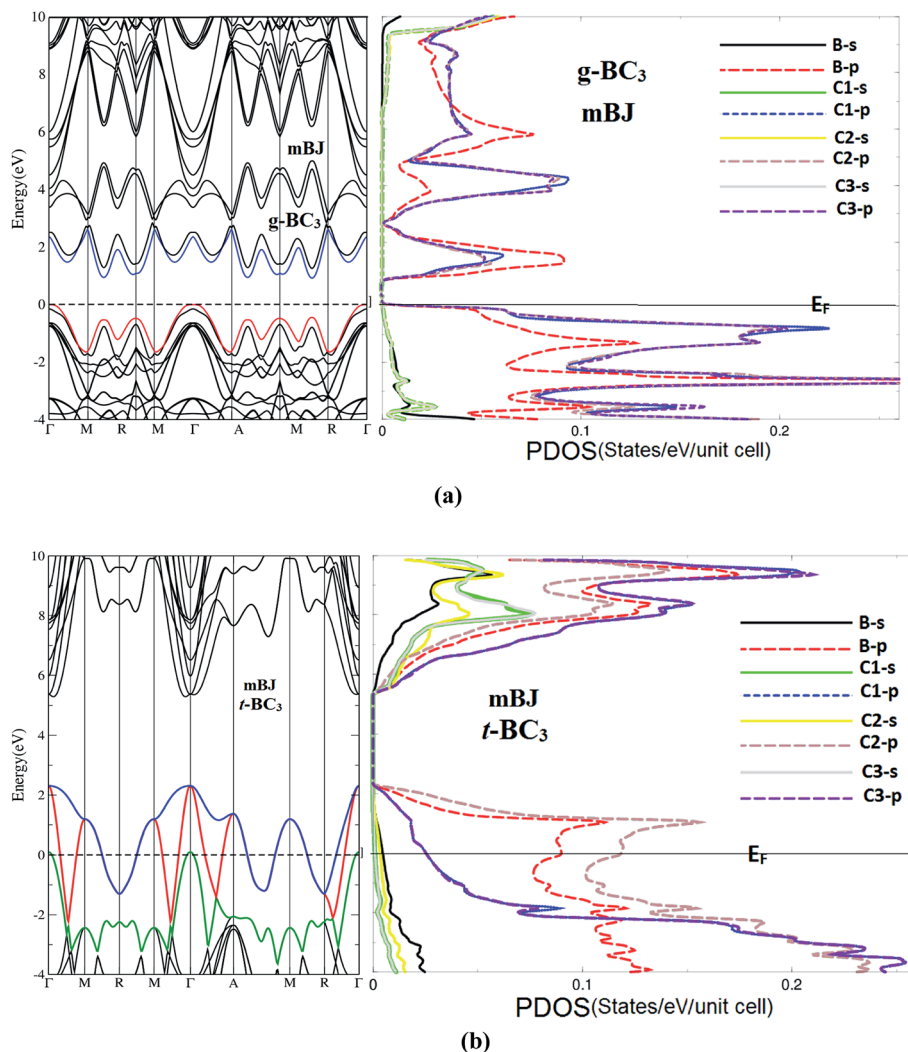


Fig. 2 (a and b) The calculated electronic band structure and density of states (B-s/p and C1,2,3 s/p states) for g-BC₃ and t-BC₃ phases. For g-BC₃ phase the conduction band maximum is highlighted by red color and the valence band minimum by blue color just for identification. White for t-BC₃ phase the three bands which cross the Fermi level are highlighted.

coefficients as a function of temperature and chemical potential are given somewhere else.^{30,43} To gain high thermoelectric efficiency, it is important that the material possess high electrical conductivity, large Seebeck coefficient and low thermal conductivity.⁴⁴

3. Results and discussion

3.1. Salient features of the electronic band structures

We recall the main features of the electronic band structure dispersion and the density of states (DOS) of g-BC₃ and t-BC₃ phases which are calculated within mBJ approach as shown in Fig. 1(a) and (b). The electronic band structure and DOS exhibit that g-BC₃ phase is a narrow band indirect band gap semiconductor, the calculated band gap is about 0.9 eV using mBJ which is much better than our EVGGA (0.7 eV) and the previous results (0.66 eV) using LDA,⁴⁵ it is well known that LDA underestimated the band gap by around 30–40%. To the best of our knowledge, there are no experimental data for the energy band

gap is available in literature to make a meaningful comparison. We would like to mention here that in our previous works^{46–48} we have calculated the energy gap using mBJ on several systems whose energy gap are known experimentally. In these calculations we find very good agreement with the experimental data. Thus, we believe that our calculated band gap within mBJ reported in this paper would produce very accurate and reliable results. Future experimental work will testify our calculated results.

The t-BC₃ is a metallic phase where the B-2p and C-2p empty orbitals of CBC block and the C-2p empty orbitals of CCC block cuts the Fermi level (E_F). It has been found that the top of the B-2p and C-2p empty orbitals is about 2.4 eV above E_F in reasonable agreement with previous results (2.28 eV (ref. 21) and 2.7 eV (ref. 17)).

3.2. Transport properties

3.2.1. Electrical conductivity. To design good thermoelectric materials, high electrical conductivity (σ) is required. This

can be achieved if the material possess high carrier concentration (n) and/or high mobility (η) according to the formula ($\sigma = ne\eta$) where σ is directly proportional to the charge carriers density (n) and their mobility (η). The electrons and holes mobility can be defined as $\eta_e = e\tau_e/m_e^*$ and $\eta_h = e\tau_h/m_h^*$ therefore, a small effective masses are required to gain high mobility.

Fig. 3(a) and (b) demonstrate the charge carriers concentration of g-BC₃ and t-BC₃ phases as a function of temperature at a certain value of the chemical potential (μ). For the semiconductor phase (g-BC₃) the charge carrier concentration is almost linearly dependent on temperature. The lowest value charge carriers concentration is about 0.002 e per uc occurs at 50 K, whereas the highest value is about 0.046 e per uc at 900 K. The high value of the carrier concentration is attributed to the fact that firstly, in g-BC₃ phase, the B-2p and C-2p orbitals lie near E_F resulting in large density of states near E_F and hence increase the scattering which lead to lower the carrier mobility, the other reason for lower the carrier mobility is the non-parabolic conduction bands near E_F (see Fig. 1). Secondly, due to the electro-negativity difference between C (2.55) and B (2.04) atoms therefore, there exists a strong covalent bonding between B-C and C-C atoms, generally covalent bond is more favorable for the transport of carriers compared with ionic component.⁴⁹ The charge carriers concentration of t-BC₃ phase is about 0.0014 e per uc at 50 K (Fig. 3(b)). Then the carriers concentration increases with increasing the temperature to reach its maximum of about 0.0018 e per uc at 200 K. Above this temperature the carriers concentration rapidly decreases with rising the temperature to reach about 0.00024 e per uc at 900 K.

The low values of the charge carrier concentration in t-BC₃ phase is attributed to the fact that since the B-2p and C-2p empty orbitals of CBC block and the C-2p empty orbitals of CCC block cuts the Fermi level, this cause to intensifying lowering the carrier concentration. The total carrier concentration is defined as the difference between the hole and the electron concentration. The electron and holes carrier concentration are define as:⁵⁰

$$h = \frac{2}{\Omega} \int_{\text{BZ}} \int_{\text{VB}} [1 - f_0(T, \varepsilon, \mu)] d\varepsilon \quad (1)$$

$$e = \frac{2}{\Omega} \int_{\text{BZ}} \int_{\text{CB}} f_0(T, \varepsilon, \mu) d\varepsilon \quad (2)$$

In the above equations, the integral is performed over the Brillouin Zone (BZ) as well as over conduction band (CB) for electrons (e) or valence band (VB) for holes (h).

The electrical conductivity of g-BC₃ and t-BC₃ phases as a function of temperature are presented in Fig. 3(c) and 3(d). It has been found that the electrical conductivity of g-BC₃ phase increases (almost) linearly with increasing the temperatures that is attributed to the fact that g-BC₃ possess high carriers concentration which increases linearly with rising the temperatures. The electrical conductivity value is about $0.2 \times 10^{18} (\Omega \text{ m s})^{-1}$ at 50 K and $5.9 \times 10^{18} (\Omega \text{ m s})^{-1}$ at 900 K. Whereas the electrical conductivity of t-BC₃ phase show the highest value of about $1.06 \times 10^{20} (\Omega \text{ m s})^{-1}$ at 50 K, then a rapid decreases occur with

increasing the temperature up to 250 K and then stays roughly constant above this temperature to reach its lowest value of about $0.994 \times 10^{20} (\Omega \text{ m s})^{-1}$ at 900 K. It is clear that the t-BC₃ exhibit higher electrical conductivity than g-BC₃ phase that is attributed to the fact that the carriers of t-BC₃ phase possess higher mobility than that of g-BC₃ phase. The relaxation time is taken to be direction independent and isotropic.⁵¹

3.2.2. Seebeck coefficient. Seebeck coefficient (S) is related to the electronic structure of the materials. The sign of S indicates the type of dominant charge carrier, positive S represent the p-type materials, whereas n-type materials have negative S . Fig. 3(e) and (f) illustrated the temperature dependences of Seebeck coefficients for g-BC₃ and t-BC₃ phases. It is clear that g-BC₃ and t-BC₃ phases exhibit p-type conduction as it has positive Seebeck coefficient in the whole temperature range. Fig. 3(e) exhibit that g-BC₃ possess the lowest value of Seebeck coefficient (180 (microV per K)) at 50 K than it show sharp increases with increasing the temperature up to 200 K. Above this temperature the Seebeck coefficient of g-BC₃ linearly increases with increasing the temperature to reach the maximum value of about 255 (microV per K) at 900 K. While the t-BC₃ phase exhibit the highest value of about 7.8 (microV per K) at 50 K then a sharp decreases occur with increasing the temperature up to 350 K and then stay roughly constant above this temperature. In general lower carrier concentration result in higher Seebeck coefficient, and the variations of effective the masses and carrier concentration will co-affect the variation of Seebeck coefficient.

3.2.3. Power factor. The power factor is defined as ($P = S^2\sigma/\tau$), where S is the Seebeck coefficient and σ/τ is the electrical conductivity. The variations of S and σ/τ helps to improve the power factor. Fig. 3(g) and (h) illustrate the power factor of g-BC₃ and t-BC₃ phases. The g-BC₃ phase exhibit almost linearly dependent power factor with temperature. At 50 K power factor of g-BC₃ is about $0.1 \times 10^{11} (\text{mW mK}^{-2})$ which increases rapidly to reach the maximum value of about $3.8 \times 10^{11} (\text{mW mK}^{-2})$ at 900 K. Whereas the power factor of t-BC₃ phase show very high value at low temperature (50 K) of about $6.0 \times 10^{10} (\text{mW mK}^{-2})$, then its drop to the lower value at 200 K to be $0.001 \times 10^{10} (\text{mW mK}^{-2})$. Above this temperature the power factor of t-BC₃ become a zero along the whole temperature range. It is clear that g-BC₃ phase show higher power factor that that of t-BC₃ phase. The power factor comes as a numerator in the figure of merit relation ($ZT = S^2\sigma T/\kappa_e$), therefore it is very important quantity for calculating the transport properties of the materials.

3.2.4. Electronic thermal conductivity. Efficient thermoelectric materials, is the materials which possess low thermal conductivity. The low thermal conductivity is required to maintain the temperature gradient. In general, the thermal conductivity ($k = k_e + k_l$) consist of two parts, the electronic part which correspond to electrons and holes that transporting heat and phonon part which correspond to phonons traveling through the lattice, BoltzTraP calculates only the electronic part. Fig. 3(i) and (j) demonstrate the electronic thermal conductivity as a function of temperature at certain value of chemical potential for g-BC₃ and t-BC₃ phases. It is clear that the electronic thermal

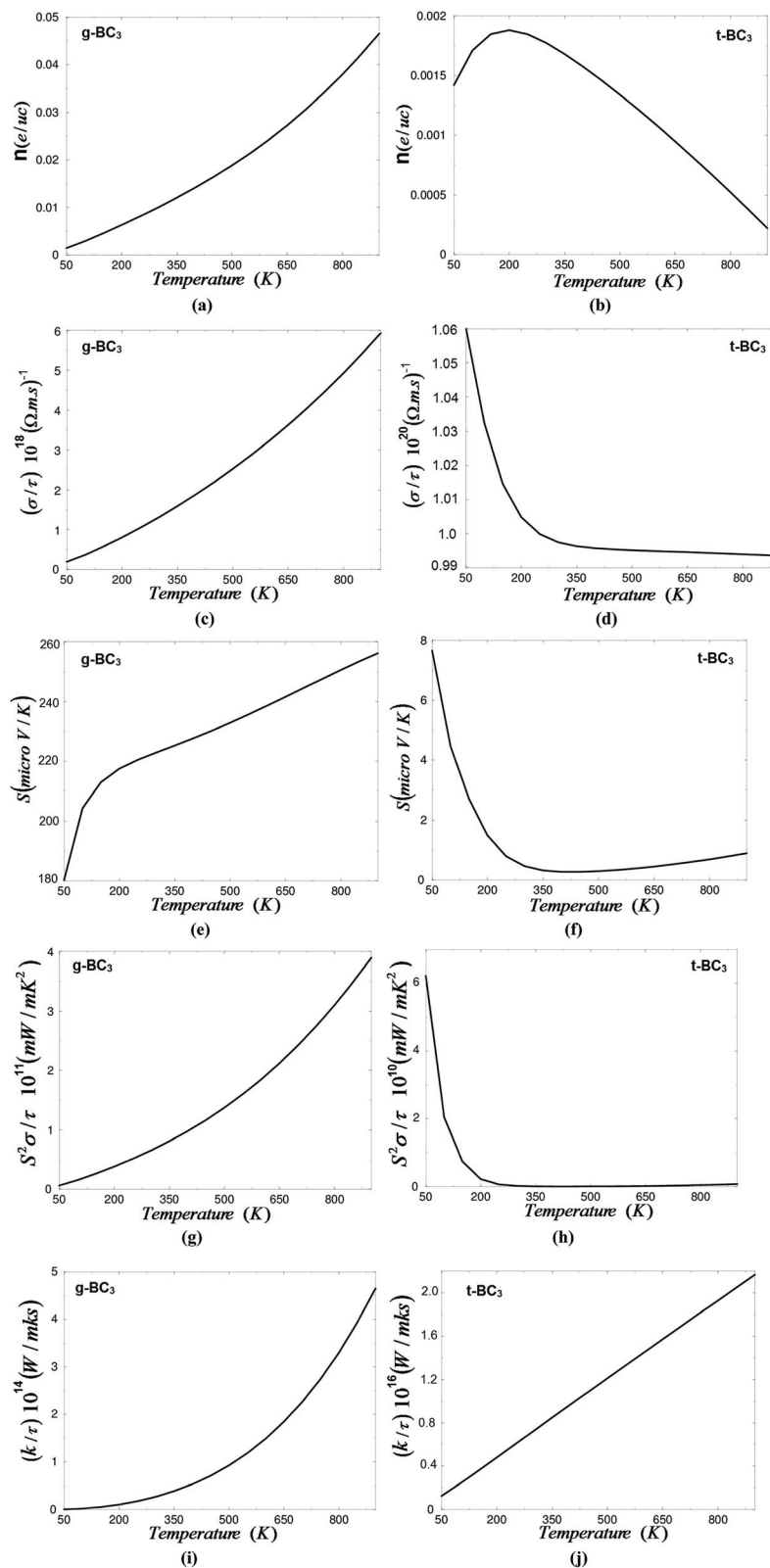


Fig. 3 The calculated transport properties as a function of temperature at certain value of chemical potential; (a and b) carrier concentration (c and d) Electrical conductivity; (e and f) Seebeck coefficient; (g and h) power factor; (i and j) electronic thermal conductivity.

conductivity of g-BC₃ is exponentially increases with increasing the temperature. It has zero value at 50 K and the highest value 4.6×10^{14} (W m⁻¹ K⁻¹ s⁻¹) at 900 K. The t-BC₃ exhibit linearly

dependent electronic thermal conductivity with temperature. At low temperature (50 K) the electronic thermal conductivity of t-BC₃ is about 0.15×10^{16} (W m⁻¹ K⁻¹ s⁻¹) while it is

2.1×10^{16} ($\text{W m}^{-1} \text{K}^{-1} \text{s}^{-1}$) at 900 K. It is clear that g-BC₃ phase exhibit lower electronic thermal conductivity than t-BC₃ phase.

4. Conclusions

The electronic transport coefficients of g-BC₃ and t-BC₃ phases are evaluated by using the semi-classical Boltzmann theory and rigid band model based on the density functional theory within the full potential linear augmented plane wave plus local orbitals (FP-LAPW + lo) method in a scalar relativistic version as embodied in the WIEN2k code. The exchange and correlation potential was treated within the modified Becke–Johnson potential which allows the calculation of band gaps with accuracy similar to the very expensive GW calculations. It has been found that the charge carrier concentration and electrical conductivity of g-BC₃ phases are systematically increases with increasing the temperature, while for t-BC₃ phase the charge carrier concentration increases with the temperature up to 200 K then a rapid decreases occurs and the electrical conductivity rapidly decreases with increasing the temperature up to 250 K and then stays roughly constant. The calculation explored that both of g-BC₃ and t-BC₃ phases are a p-type conduction. The calculation show that the g-BC₃ phase exhibit higher Seebeck coefficient, higher power factor and low electronic thermal conductivity than t-BC₃ phase. Based on the above results we expected that the g-BC₃ phase exhibit better thermoelectric properties than that of t-BC₃ phase.

Acknowledgements

The result was developed within the CENTEM project, reg. no. CZ.1.05/2.1.00/03.0088, cofunded by the ERDF as part of the Ministry of Education, Youth and Sports OP RDI programme and, in the follow-up sustainability stage, supported through CENTEM PLUS (LO1402) by financial means from the Ministry of Education, Youth and Sports under the National Sustainability Programme I. Computational resources were provided by MetaCentrum (LM2010005) and CERIT-SC (CZ.1.05/3.2.00/08.0144) infrastructures.

References

- 1 H. Wang, W. Chu and H. Jin, *Comput. Mater. Sci.*, 2012, **60**, 224.
- 2 K. P. Ong, D. J. Singh and P. Wu, *Phys. Rev. B: Condens. Matter Mater. Phys.*, 2011, **83**, 115110.
- 3 D. Parker and D. J. Singh, *Phys. Rev. B: Condens. Matter Mater. Phys.*, 2011, **83**, 233206.
- 4 D. Parker, M.-H. Du and D. J. Singh, *Phys. Rev. B: Condens. Matter Mater. Phys.*, 2011, **83**, 245111.
- 5 D. J. Singh, *Phys. Rev. B: Condens. Matter Mater. Phys.*, 2010, **81**, 195217.
- 6 K. P. Ong, D. J. Singh and P. Wu, *Phys. Rev. Lett.*, 2010, **104**, 176601.
- 7 G. B. Wilson-Short, D. J. Singh, M. Fornari and M. Suewattana, *Phys. Rev. B: Condens. Matter Mater. Phys.*, 2007, **75**, 035121.
- 8 D. J. Singh and D. Kasinathan, *J. Electron. Mater.*, 2007, **36**, 736.
- 9 D. J. Singh, *Phys. Rev. B: Condens. Matter Mater. Phys.*, 2007, **76**, 085110.
- 10 D. J. Singh, *Mater. Res. Soc. Symp. Proc.*, 2008, **1044**, U02–U05.
- 11 D. J. Singh, *US Pat.* 8,487,178, 2013.
- 12 H. A. Rahnamaye Aliabad, M. Ghazanfari, I. Ahmad and M. A. Saeed, *Comput. Mater. Sci.*, 2012, **65**, 509.
- 13 F. J. DiSalvo, *Science*, 1999, **285**, 703–706.
- 14 T. M. Trit, *Science*, 1996, **272**, 1276–1277.
- 15 L. E. Bell, *Science*, 2008, **321**, 1457–1461.
- 16 P. V. Zinin, L. C. Ming, I. Kudryashov, N. Konishi and S. K. Sharma, *J. Raman Spectrosc.*, 2007, **38**, 1362.
- 17 Z. Liu, J. He, J. Yang, X. Guo, H. Sun, H.-T. Wang, E. Wu and Y. Tian, *Phys. Rev. B: Condens. Matter Mater. Phys.*, 2006, **73**, 172101.
- 18 R. Hoffmann, R. Hoffmann, T. Hughbanks, M. Kertesz and P. H. Bird, *J. Am. Chem. Soc.*, 1983, **105**, 4831.
- 19 C. J. Pickard, V. Milman and B. Winkler, *Diamond Relat. Mater.*, 2001, **10**, 2225.
- 20 J. L. He, L. C. Guo, E. Wu, X. G. Luo and Y. J. Tian, *J. Phys.: Condens. Matter*, 2004, **16**, 8131.
- 21 M. M. Ali, A. K. M. A. Islam, M. Aftabuzzaman and F. Parvin, *J. Sci. Res.*, 2010, **2**(2), 203–213.
- 22 P. V. Zinin, L. C. Ming, S. K. Sharma, S. M. Hong, Y. Xie, T. Irifune and T. Shinmei, *J. Phys.: Conf. Ser.*, 2008, **121**, 062002.
- 23 H. Liu, Q. Li, L. Zhu and Y. Ma, *Phys. Lett. A*, 2011, **375**, 771–774.
- 24 L. Li, W. X. Li, D. Han, S. Wei Xin, Y. Yang, W. Zhou and Y. Feng Lu, *Mater. Sci. Forum*, 2013, **749**, 551.
- 25 E. A. Ekimov, V. A. Sidorov, E. D. Bauer, N. N. Mel'nik, N. J. Curro, J. D. Thompson and S. M. Stishov, *Nature*, 2004, **428**, 542.
- 26 Y. Ma, J. S. Tse, T. Cui, D. D. Klug, L. Zhang, Y. Xie, Y. Niu and G. Zou, *Phys. Rev. B: Condens. Matter Mater. Phys.*, 2005, **72**, 014306.
- 27 Y. Takano, T. Takenouchi, S. Ishii, S. Ueda, T. Okutsu, I. Sakaguchi, H. Umezawa, H. Kawarada and M. Tachiki, *Diamond Relat. Mater.*, 2007, **16**, 911.
- 28 K. W. Lee and W. E. Pickett, *Phys. Rev. Lett.*, 2004, **93**, 237003.
- 29 A. H. Reshak, *Phys. Chem. Chem. Phys.*, 2015, **17**, 8006.
- 30 G. K. H. Madsen and D. J. Singh, BoltzTraP. A code for calculating band-structure dependent quantities, *Comput. Phys. Commun.*, 2006, **175**, 67–71.
- 31 A. H. Reshak and S. Auluck, *RSC Adv.*, 2014, **4**, 37411.
- 32 A. H. Reshak, *RSC Adv.*, 2014, **4**, 39565.
- 33 M. Jamal, N. Kamali Sarvestani, A. Yazdani and A. H. Reshak, *RSC Adv.*, 2014, **4**, 57903.
- 34 A. H. Reshak, *RSC Adv.*, 2015, **5**, 22044.
- 35 P. Blaha, K. Schwarz, G. K. H. Madsen, D. Kvasnicka and J. Luitz, *WIEN2k, An augmented plane wave plus local orbitals program for calculating crystal properties*, Vienna University of Technology, Austria, 2001.
- 36 J. P. Perdew, S. Burke and M. Ernzerhof, *Phys. Rev. Lett.*, 1996, **77**, 3865.

- 37 W. Kohn and L. J. Sham, *Phys. Rev. A*, 1965, **140**, 1133.
- 38 E. Engel and S. H. Vosko, *Phys. Rev. B: Condens. Matter Mater. Phys.*, 1993, **47**, 13164.
- 39 F. Tran and P. Blaha, *Phys. Rev. Lett.*, 2009, **102**, 226401.
- 40 B. G. Janesko, *J. Chem. Phys.*, 2011, **134**, 184105.
- 41 B. M. Wong and J. G. Cordaro, *J. Phys. Chem. C*, 2011, **115**, 18333.
- 42 D. Wang, L. Tang, M. Q. Long and Z. G. Shuai, *J. Chem. Phys.*, 2009, **131**, 224704.
- 43 T. J. Scheidemantel, C. Ambrosch-Draxl, T. Thonhauser, J. V. Badding and J. O. Sofo, Transport coefficients from first-principles calculations, *Phys. Rev. B: Condens. Matter Mater. Phys.*, 2003, **68**(6), 125210.
- 44 G. J. Snyder and E. S. Toberer, Complex thermoelectric materials, *Nat. Mater.*, 2008, **7**, 105–114.
- 45 A BC₃ monolayer in an unrelaxed graphite structure with $d_{BC} = d_{CC} = 1.42 \text{ \AA}$ is calculated to be an indirect-gap semiconductor with a negligibly small gap. This gap opens upon structural relaxation. In general, the true gap is larger than the calculated LDA gap, as discussed, *e.g.*, by M. S. Hybertsen and S. G. Louie, *Phys. Rev. B: Condens. Matter Mater. Phys.*, 1986, **34**, 5390.
- 46 A. H. Reshak, H. Huang, H. Kamarudin and S. Auluck, *J. Appl. Phys.*, 2015, **117**, 085703.
- 47 A. H. Reshak, O. V. Parasyuk, A. O. Fedorchuk, H. Kamarudin, S. Auluck and J. Chyský, *J. Phys. Chem. B*, 2013, **117**, 15220–15231.
- 48 A. H. Reshak, I. V. Kityk, O. V. Parasyuk, H. Kamarudin and S. Auluck, *J. Phys. Chem. B*, 2013, **117**, 2545–2553.
- 49 G. J. Snyder and E. S. Toberer, *Nat. Mater.*, 2008, **7**, 105–114.
- 50 A. H. Reshak and W. Khan, *J. Alloys Compd.*, 2014, **591**, 362–369.
- 51 B. Xu, X. Li, G. Yu, J. Zhang, S. Ma, Y. Wang and L. Yi, *J. Alloys Compd.*, 2013, **565**, 22–28.